# Modeling and optimization of mass-limited targets for EUV Lithography

**T. Sizyuk and A. Hassanein**

**Center for Materials under Extreme Environment, School of Nuclear Engineering**
**Purdue University, West Lafayette, IN, USA**

## ABSTRACT

Current challenges in the development of efficient laser produced plasma (LPP) sources for EUV lithography are increasing EUV power at IF and maximizing lifetime and therefore, reducing cost of devices. Mass-limited targets such as small tin droplets are considered among the best choices for cleaner operation of the optical system because of lower mass of atomic debris produced by the laser beam. The small diameter of droplets, however, decreases the conversion efficiency (CE) of EUV photons emission, especially in the case of $CO_2$ laser, where laser wavelength has high reflectivity from the tin surface.

We investigated ways of improving CE in mass-limited targets. We considered in our modeling various possible target phases and lasers configurations: from solid/liquid droplets subjected to laser beam energy with different intensities and laser wavelength to dual-beam lasers, i.e., a pre-pulse followed by a main pulse with adjusted delay time in between. We studied the dependence of vapor expansion rate, which can be produced as a result of droplet heating by pre-pulse laser energy, on target configuration, size, and laser beam parameters. As consequence, we studied the influence of these conditions and parameters on the CE and debris mass accumulation.

For better understanding and more accurate modeling of all physical processes occurred during various phases of laser beam/target interactions, plasma plume formation and evolution, EUV photons emission and collection, we have implemented in our HEIGHTS package state-of-the art models and methods, verified, and benchmarked against laboratory experiments in our CMUXE center as well as various worldwide experimental results.

**Keywords:** EUV, LPP, HEIGHTS, Mass-limited targets, Debris mitigation, $CO_2$ laser.

## 1. INTRODUCTION

The process of heating tin droplets by laser energy results in formation of vapor (detached neutral atoms), fragments (clusters of atoms), and plasma. Final target decomposition to these elements depends on the droplet size and laser beam parameters. Small droplets with sizes of 10 - 30 μm are considered as perspective targets [1], since one of the main goals in the development of EUV source for high-volume manufacture is increasing optical components lifetime that is to minimize the debris generation and deposition in the source chamber.

However, small sizes of target leads to utilizing reasonable small spot size of the laser beam and such restriction of sizes results in: 1) increasing the relative part of laser energy for initial heating of the target, 2) delaying the processes of vaporization and plasma plume formation, 3) reducing the size of EUV source area and, therefore, decreasing the brightness of source, and 4) loss of the plasma geometrical containment [2]. As a result, small spherical targets give significantly lower CE, especially in the case of $CO_2$ laser - approximately two times less in comparison with the planar targets heated by the laser with larger spot.

Dual-pulse systems can be used for increasing CE of EUV source from small spherical targets. In this regard we can consider two modes for utilizing prepared target matter. The first one is based on the heating by the main laser of plasma plume created at the pre-pulse stage and expanded during the short time, up to 100 ns [3][4]. The second one is related to utilizing the evaporated and fragmented parts of the droplet [1]. Heating of this matter is reasonable after delay in the μs

Extreme Ultraviolet (EUV) Lithography III, edited by Patrick P. Naulleau,
Obert R. Wood II, Proc. of SPIE Vol. 8322, 83222K · © 2012 SPIE
CCC code: 0277-786X/12/$18 · doi: 10.1117/12.916432

range, since velocities of this components is 10-100 times lower than plasma velocity [5] and spatial expansion of such matter to areas covered by the larger plasma spot requires longer time.
In this work we initially modeled the evaporation rate of small droplet in dependence on the pre-pulse laser wavelength. Then, we modeled plasma/vapor expansion developed from the most vaporized target (80% of 30 μm droplet), optimizing delay between pre-pulse and main pulse and then adjusting spot size of the main, $CO_2$, laser to get efficient conditions for EUV photons output. Such detailed simulations were possible with our comprehensive and advanced models for the description of plasma physics processes. Our HEIGHTS package contains detail models for energy deposition, vapor/plasma formation/evolution and magneto hydrodynamic (MHD), thermal conduction in material and in plasma, atomic physics and resulting opacities, detailed photon radiation transport, and interaction between plasma/radiation and target material. These models were described in several publications [6]-[8]. Below we give brief description of the implemented model for target vaporization since it is important in this particular study.

## 2. TARGET VAPORIZATION MODEL

HEIGHTS package includes model for tin target vaporization based on the kinetics of evaporation. The model establishes the connection between the surface temperature and the net atom flux leaving the surface taking into account the possibility of recondensation [9]. The time-dependent net evaporation rate may be approximated by:

$$J(T) = J_e^{eq}, \quad if\ t < t_v$$
$$J(T) = J_e^{eq}[0.8 + 0.2\exp(-(t - t_v)/10\tau_c)], \quad if\ t > t_v$$

where $\tau_c$ is the above-surface vapor collision time; $t_v$ is the preheat time for preparing the vapor zone when recondensation become significant; $J_e^{eq}$ is the equilibrium evaporation flux which can be estimated as:

$$J_e^{eq}(T) = 5.8\times10^{-2}\,\frac{\alpha\sqrt{A}P_v(T_v)}{\rho(T_v)\sqrt{T_v}}$$

where $\alpha$ is the sticking probability; $A$ is the atomic mass; $P(T_v)$ is the saturated vapor pressure; $\rho(T_v)$ is the density at the surface; and $T_v$ is the vapor temperature.
In our simulations this surface vaporization process interplays with Monte Carlo modeling of laser photons absorption and reflection in liquid/vapor/plasma as well as photon transport in plasma. Vaporized layer above the target surface initializes process of laser photons absorption in vapor/plasma that prevents their penetration to the target surface. At the same time, radiated plasma photons add their energy to the heating of droplet and this energy load to the target can be significant from the well-developed hot plasma plume.

## 3. INFLUENCE OF LASER WAVELENGTH AND INTENSITY ON VAPORIZATION DYNAMICS

The mechanisms described above in the formation of laser-produced plasma (LPP) allow prediction of vaporization rate with acceptable accuracy. For the considered time of the pre-pulse laser duration, 10 ns, we can neglect possible target fragmentation and fragments distribution.

Figures 1 and 2 illustrate the process of pre-plasma creation, i.e., vaporization and plasma formation by the pre-pulse lasers with two different wavelengths and with the same other parameters such as 10 ns pulse duration and $10^{10}$ W/cm$^2$ intensity, 30 μm spot on 30 μm droplet. Tin droplet with this size has mass of $10^{-7}$ g and laser beam with 266 nm wavelength and this intensity only vaporized one third of the droplet. Dependence of vaporization rate on the wavelength has nonlinear tendency since this process, in self-consistent simulation, depends on 1) the time of initiation of laser energy absorption in plasma that reduces energy load to the target; 2) geometry of target, since heating of the droplet by the laser and by the plasma itself can cause vaporization from the sides of droplet. Figure 3(a) shows evaporated mass during the laser beam pulse for two laser wavelengths. Figure 3(b) illustrates dependence of droplet vaporization, of the 1064 nm wavelength laser, on the intensity indicating less vaporized mass by more intensive laser beam.

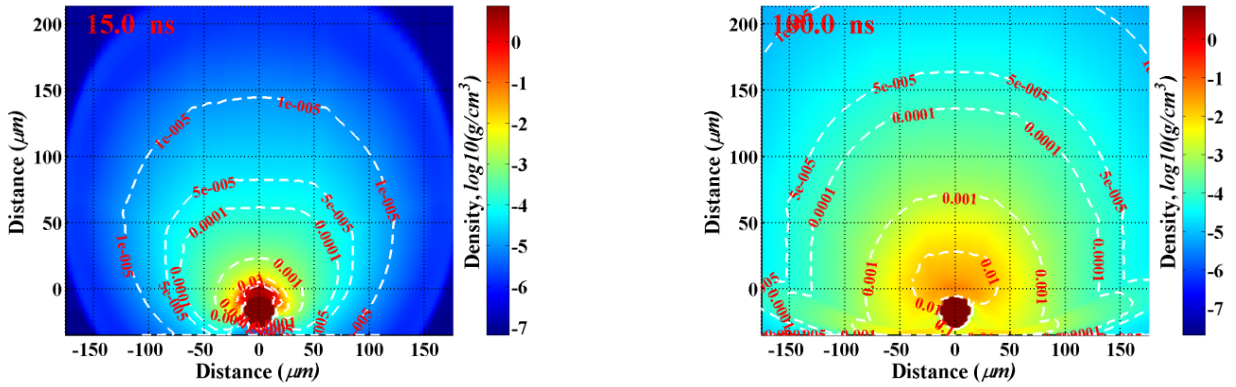


Fig.1. Mass density distributions at the end of pre-pulse laser (left) and after 100 ns delay (right). Pre-plasma was created by the laser beam with 1064 nm wavelength and intensity of $10^{10}$ W/cm$^2$.

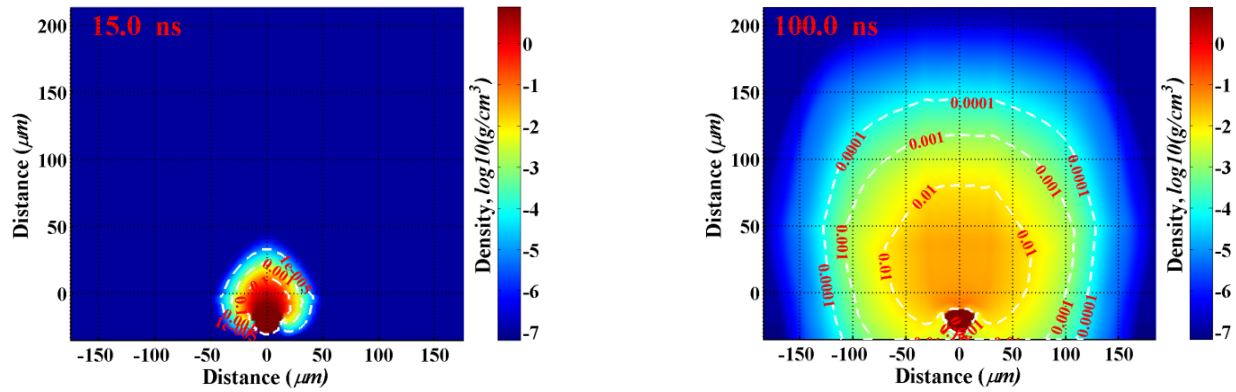


Fig.2. Mass density distributions at the end of pre-pulse laser (left) and after 100 ns delay (right). Pre-plasma was created by the laser beam with 266 nm wavelength and intensity of $10^{10}$ W/cm$^2$.

With the same other laser and target parameters, laser with longer wavelength created warmer plasma that was expanded faster (Figs. 1 and 2), however it vaporized less mass that results in less dense plasma/vapor plume developed during 100 ns.

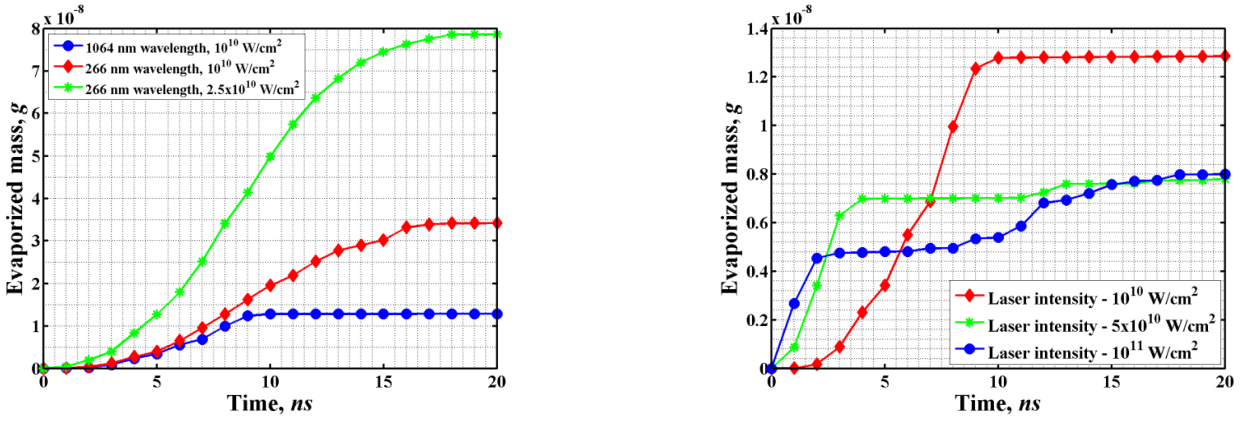


a) b)

Fig.3. Dependence of evaporation dynamics on pre-pulse laser wavelength and laser beam intensity a) wavelength dependence at different intensities and b) laser intensity dependence at 1064 nm wavelength. Laser beam parameters used are 30 μm spot size and 10 ns duration.

## 4. PLASMA TEMPERATURE, DENSITY AND EUV SOURCE LOCATION

The implemented models in HEIGHTS Monte Carlo description for the radiation transport include detailed calculation of opacities that allow precise prediction of EUV source location and strength based on the fundamental description of plasma radiation processes without any adjustments parameters or correlations. These models were benchmarked against CMUXE experimental results [2] as well as with other extensive experimental studies, e.g., by Spitzer, et al. [10], [11], for various laser beam parameters. We analyzed the dependence of source location and intensity on plasma conditions created by Nd:YAG and $CO_2$ lasers, and on plasmas heated after the pre-pulse.

Figures 4 (a) and (b) show that optimum temperature for EUV output is around 30-40 eV in plasmas created by both lasers. Since the 10 μm wavelength is absorbed in region with plasma density of $10^{19}$ $cm^{-3}$, location of maximum EUV output is determined by this density value. Laser with 1064 nm wavelength is absorbed by plasma with density $10^{20}$ -$10^{21}$ $cm^{-3}$ near the target surface, that also determines the location of EUV source. We used in these simulations the optimized intensities for lasers with considered spot size (30 μm), such as $5x10^{10}$ $W/cm^2$ for $CO_2$ and $10^{11}$ $W/cm^2$ for Nd:YAG.

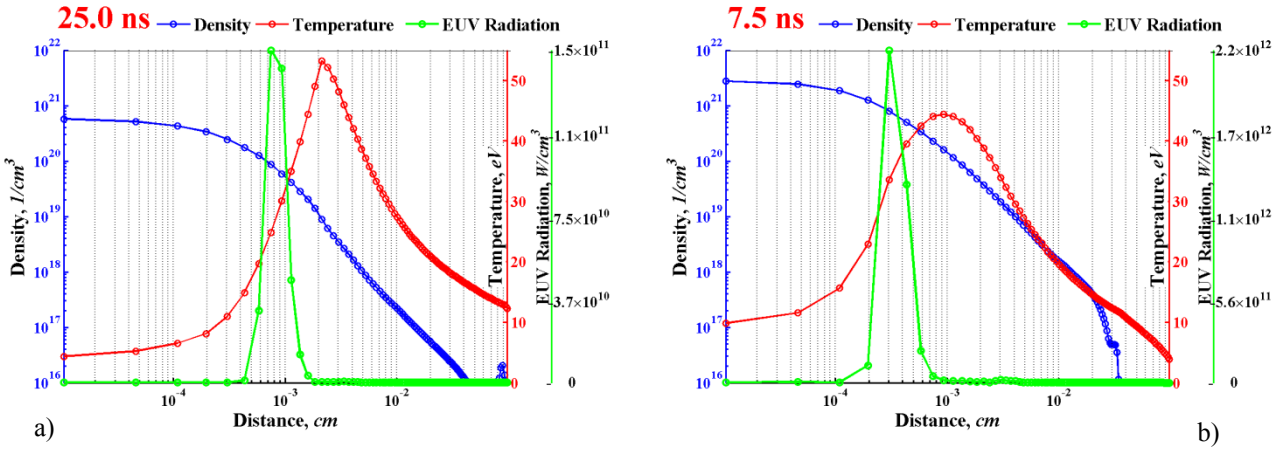


Fig.4. EUV source location and intensity in relation with density and temperature of plasma created by: a) $CO_2$ laser; b) Nd:YAG laser.

Figures 4 (a) and (b) show also that intensity of EUV source in denser plasma (created by Nd:YAG) is one order of magnitude higher. It is explained by the optical properties of tin plasma with high EUV emissivity at specific temperature values (30-40 eV), where EUV emission (and correspondingly absorption) is increased significantly with density increase, however emission (and absorption also) is decreased suddenly at higher temperature values, located above EUV source. Figures 5 (a) and (b) illustrate EUV energy distribution for the described above cases. Radiation fluxes in plasma created by Nd:YAG laser are one order of magnitude larger; resulting EUV radiation power, reached the walls of the modeled chamber or the collecting location, is several times higher.

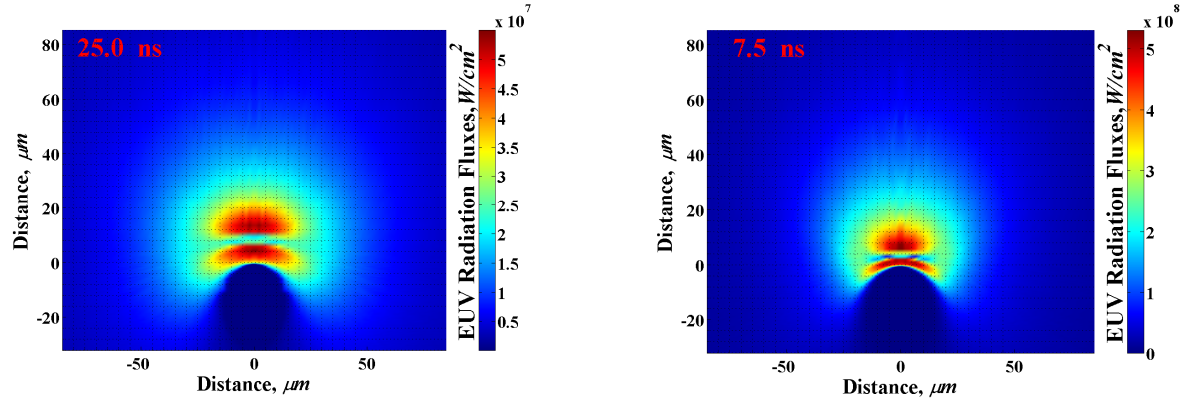


Fig.5. EUV radiation fluxes in plasma created by: a) $CO_2$ laser; b) Nd:YAG laser.

In these cases modeling was done for 30 μm Tin droplet. We obtained 1.3% CE for Nd:YAG laser and 0.45% for $CO_2$. The high reflectivity of the 10 μm laser and the small spot size are reasons of the low EUV intensity source and the small volume of EUV emitting area, created by this wavelength that also results in very low efficiency. Pre-plasma created by shorter wavelength extends the area suitable for $CO_2$ wavelength absorption. Figures 6 (a) and (b) show location and intensity of EUV power collected in 2π sr during 70 ns from the plasma created by $CO_2$ laser without (a) and with pre-pulse (b). In the second case pre-plasma was created by 266 nm wavelength and expanded during 100 ns before the main pulse impacted. For this case we obtained 1.7% CE.

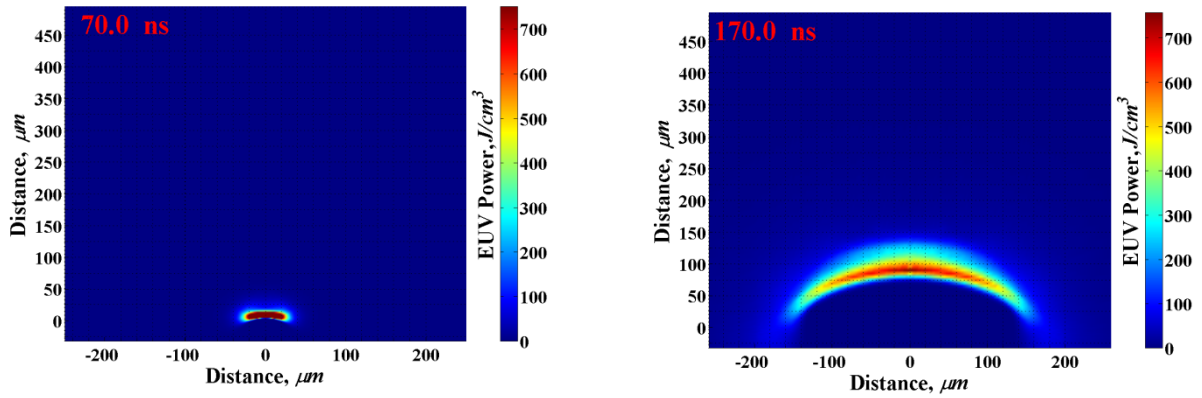


a) b)

Fig.6. EUV source collected in 2π sr during 70 ns: a) $CO_2$ laser without pre-plasma; b) $CO_2$ laser after pre-plasma.

## 5. MODELING RESULTS FOR PERFECTLY VAPORIZED TARGET

Laser beam with 266 nm wavelength and intensity of $2.5 \times 10^{10}$ W/cm$^2$ vaporized 80% of 30 μm droplet (Fig. 3a). To evaluate the efficiency of the prepared plasma/vapor plume for EUV photons output we used the same $CO_2$ laser intensity, $7.5 \times 10^9$ W/cm$^2$, and pulse duration, 30 ns. We varied delay time and spot size of the main laser. Figure 7 shows results of optimization of these two parameters. The CE from 30 μm droplet with $CO_2$ and Nd:YAG laser without pre-pulse are given for comparison.

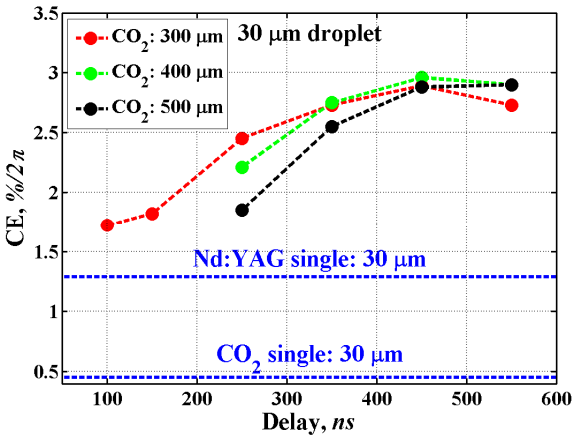


Fig.7. CE from 30 μm droplet as function of delay between pulses and spot size of $CO_2$ laser.

## CONCLUSION

Optimization of EUV sources from small droplet targets using dual laser pulses depends on many parameters and requires detailed analyses of pre-plasma conditions. HEIGHTS comprehensive simulation package, used in this analysis, includes detail models for energy deposition, vapor/plasma formation/evolution and magneto hydrodynamic (MHD), thermal conduction in material and in plasma, atomic physics and resulting opacities, detailed photon radiation transport, and interaction between plasma/radiation and target material. For 1064 nm pre-pulse laser, tin evaporation rate decreased with increasing laser beam intensity from $10^{10}$ to $10^{11}$ W/cm$^2$, utilizing the same spot size as droplet diameter. Laser with 266 nm wavelength, penetrating deeper to the target, created denser but colder plasma/vapor plume that required more time for expansion to be efficient for the absorption of the 10 μm wavelength. Overall, efficient EUV source depends on combination of various parameters including pre-pulse laser wavelength/intensity, initial size of target/vaporization rate, and delay time/spot size.


### ACKNOWLEDGMENTS

This work is partially supported by the College of Engineering, Purdue University. We gratefully acknowledge the computing resources provided by the Fusion cluster operated by the Laboratory Computing Resource Center at Argonne National Laboratory.


## REFERNCES


[1] Mizoguchi, H., Abe, T., Watanabe, Y., Ishihara, T., Ohta, T., Hori, T., Yanagida, T., Nagano, H., Yabu, T., Nagai, S., Soumagne, G., Kurosu, A., Nowak, K.M., Suganuma, T., Moriya, M., Kakizaki, K., Sumitani, A., Kameda, H., Nakarai, H., Fujimoto, J., "100W 1st Generation Laser-Produced Plasma light source system for HVM EUV lithography", SPIE 7969 7969-08, 2011.

[2] Hassanein, A., Sizyuk, V., Sizyuk, T., Harilal, S., "Effects of plasma spatial profile on conversion efficiency of laser-produced plasma sources for EUV lithography", J. Micro/Nanolith., MEMS and MOEMS, 8(4) 041503, 2009.

[3] Hassanein, A., Sizyuk, T., Sizyuk, V., and Harilal, S. S., "Combined effects of pre-pulsing and target geometry on efficient EUV production from laser produced plasma experiments and modeling", J. Micro/Nanolith MEMS MOEMS 10, 033002 1-6 (2011).

[4] Tillack, M.S., and Tao, Y., "Optimization of laser-produced plasma light sources for EUV lithography", 2011 International Workshop on EUV Lithography, Maui, HI, June, 2011.

[5] Endo, A., "Physical aspects of pre-pulsed tin droplet in transport magnetic field", 2011 International Workshop on EUV and Soft X-Ray Sources, Ireland, November 7-10, 2011.

[6] Sizyuk, V., Hassanein, A., and Sizyuk, T., "Three-dimensional simulation of laser-produced plasma for extreme ultraviolet lithography applications", Journal of Applied Physics, 100 103106, 2006.

[7] Sizyuk, V., Hassanein, A., and Bakshi, V., "Modeling and optimization of debris mitigation systems for laser and discharge-produced plasma in EUV lithography devices", J. Micro/Nanolith., MEMS and MOEMS, 6 043003, 2007.

[8] Sizyuk, V., Hassanein, A., Morozov, V., Tolkach, V., Sizyuk, T., "Numerical simulation of laser-produced plasma devices for EUV lithography using the HEIGHTS integrated model", Numerical heat transfer, Part A, 49 215-236, 2006.

[9] Hassanein, A., Kulcinski, G.L., and Wolfer, W.G., "Surface melting and evaporation during disruptions in magnetic fusion reactors", Nuclear Engineering and Design-Fusion 1**,** 307-324, 1984.

[10] Sizyuk, V., Hassanein, A., and Sizyuk, T., "Hollow laser self-confined plasma for EUV lithography and other applications", Laser and Particle Beams 25, 143-154, 2007.

[11] Spitzer, R.C., Orzechowski, T.J., Phillion, D.W., Kauffman, R.L., and Cerjan, C., J. Appl. Phys. 79, 2251, 1996.